Kinetik: Game Technology, Information System, Computer Network, Computing, Electronics, and Control
Journal homepage: http://kinetik.umm.ac.id
ISSN: 2503-2267
Vol. 11, No. 1, February, Pp. 135-148

ANFIS-controlled high step-up DC DC converter for fuel cell systems with enhanced efficiency against load variation

Harmini*[1], Mochamad Ashari[2], Feby Agung Pamuji[2]
Department of Electrical Engineering, Universitas Semarang, Semarang, Indonesia[1]
Department of Electrical Engineering, Institut Teknologi Sepuluh Nopember, Surabaya, Indonesia [2]

Article Info
Keywords:
High Step-up DC-DC Converter, ANFIS control system, Fuel Cell System

Article history:
Received: August 01, 2025
Accepted: October 24, 2025
Published: February 01, 2026

Cite:
H. Harmini, M. Ashari, and F. A. Pamuji, "ANFIS-Controlled High Step-Up DC DC Converter for Fuel Cell Systems with Enhanced Efficiency Against Load Variation", KINETIK, vol. 11, no. 1, Feb. 2026.
https://doi.org/10.22219/kinetik.v11i1.2456

*Corresponding author.
Harmini
E-mail address:
harmini@usm.ac.id

Abstract
The primary challenge in utilizing Fuel Cell (FC) systems lies in their inherently low and fluctuating output voltage, which contrasts with the requirements of a Direct Current (DC) bus network that demands a stable and relatively high voltage level. Ensuring consistent voltage regulation in the DC bus network is essential for reliable system performance. An interface converter is required to elevate and stabilize the voltage output under dynamic operating conditions. This paper introduces a high step-up DC–DC converter integrated with an Adaptive Neuro-Fuzzy Inference System (ANFIS)-based control scheme for enhancing the performance of FC power systems. The proposed work encompasses the modeling, analytical design, and structural development of the converter and its intelligent control mechanism. The proposed high step-up converter exhibits a novel structural configuration that integrates a clamp unit, a Multiplier Cell (MC), and cascaded Quadratic Boost Converter (QBC) stages. The contribution of this converter topology lies in its ability to enhance the reliability of fuel cell–based renewable energy systems, achieve high voltage amplification, ensure optimal efficiency, and maintain dynamic stability. This topology is specifically developed to attain an ultra-high voltage conversion ratio, achieving a significant voltage gain of up to 9.65 times, thereby effectively increasing the input voltage from 45 V to 400 V. The ANFIS controller effectively maintains a stable output voltage of 400 V with a maximum deviation of only ±3.5%. The proposed converter achieves a peak efficiency of 87% under varying load conditions, demonstrating its suitability for fuel cell-based energy systems.

1. Introduction

The implementation of various Renewable Energy Sources (RES), such as Fuel Cells (FC) and Photovoltaics (PV), is unavoidable due to the growing scarcity of fossil fuels and the increasingly alarming state of environmental conditions[1][2][3]. However, most renewable energy sources generate low voltage about 12-24 V, which presents a significant challenge in their implementation as alternative energy solutions. One of the major technical challenges in integrating these RES technologies lies in their inherently low output voltage characteristics, particularly in Fuel Cells, which typically produce only a few volts per cell[4][5][6]. This low voltage level not only limits their direct applicability in medium or high-power system but also leads to efficiency degradation, increased converter complexity and higher power losses during voltage boosting. Consequently, effective power conditioning and high-gain DC-DC conversion are essential to ensure stable and efficient power delivery from fuel cell based renewable energy system.

A considerable amount of research has focused on integrating fuel cells into renewable energy frameworks[7], [8]. Nevertheless, the inherent drawbacks of fuel cells, particularly their low and unstable output voltage, remain insufficiently resolved. Such voltage limitations demand the implementation of DC–DC converter systems capable of providing exceptionally high voltage gain. Consequently, there is a pressing need to design a converter topology that can deliver significant voltage amplification while ensuring optimal power conversion efficiency and maintaining dynamic stability under various load and fuel cell operating conditions. A high step-up DC-DC converter is essential to function as an interface linking the power source and the load, enabling voltage level adaptation, ensuring the output voltage meets the specified standards. Conventional converters, such as boost converters, have demonstrated their capability to increase voltage levels; however, they are constrained by low efficiency and can typically achieve a voltage increase of only up to seven times[9].The integration of a traditional converter with voltage enhancement techniques is frequently used to attain higher voltage gain levels [10][11].

Several voltage-boosting techniques have been utilized, including switched capacitors, switched inductors, coupled inductors, multiplier cells, and high-frequency transformers. Additionally, Alternative techniques, including cascading and interleaving, have been investigated to improve voltage gain and suppress output current ripple in DC-

DC converter designs[7][12][13][14][15][16][17][18]. A converter with a cascade amplifier is often chosen for its simple configuration; however, it has the drawbacks of requiring numerous components, low efficiency, and a high voltage drop. Therefore, a converter with interleaving topology is preferred to reduce ripple, increase voltage gain, and minimize the voltage drop across each active component[17]. Another configuration to increase voltage is application of coupled inductor (CL)[8][19][20][21]. The combination of a coupled inductor (CL) can help suppress voltage drop across the semiconductor components. However, it introduces the issue of leakage inductance in the converter. This problem can be mitigated by incorporating a clamp circuit, which enhances the converter's efficiency and eliminates ripple caused by the semiconductor components[16][22].

Development of the cascade and interleaving converters is the Quadratic Boost Converter (QBC)[9][13][23][24][25][26]. This converter employs a standard boost converter design, allowing it to achieve a high voltage gain. The combination of the QBC with CL components and the switched capacitor technique has been presented to achieve high step-up voltage conversion[27][28][29]. The integration of the QBC with a voltage doubler, as described by[5]. Utilizes the cascade method combined with a transformer operating at high frequency. Additionally, the combination of the QBC with a Voltage Multiplier Cells (VMC) can be employed to further boosting the output voltage. This converter has been discussed in the research by[5][30].

Hybrid configurations of boost and buck-boost converters with cascade connections have been reported by[8]. However, these converters are not capable of achieving significant voltage enhancement. Research in [17] a high step-up DC-DC converter architecture that integrates two interleaved boost stages, a high-frequency isolation transformer, and a coupled inductor to enhance voltage conversion efficiency. However, this converter still struggles to achieve substantial voltage gain and relies on a large number of components, which ultimately raises the total cost. Research in [9] discusses a high step-up DC-DC converter integrated with a double boost converter, a coupled inductor, and a multiplier cell, using a constant DC voltage input source. This configuration, referred to as an ultrahigh step-up converter, is designed for low-power specifically 150 watts applications.

In [19], A high step-up DC-DC converter integrating a Dual Floating Output Boost Converter (DFOBC) topology has been developed for fuel cell power systems. This design achieves higher frequency switching, high power density, and Zero Voltage Transition (ZVT) operation, effectively minimizing switching losses. In [7] and [31], A boost converter with high quadratic voltage gain (QBC) and a high-gain non-isolated DC-DC converter employing symmetric inductor magnetization techniques have been proposed to enhance voltage step-up capabilities. These designs offer wide voltage ratios, minimal input current ripple and reduced overall voltage stress, making them well-suited for Fuel Cell Electric Vehicle (FCEV) applications. The work in [6] presented an integrated multi-mode converter using only one inductor for FCEVs. By combining two converters and incorporating Battery Mode Selection Cells (BMSCs), The system offers enhanced power density and lower core loss compared to conventional converters, ensuring higher efficiency in typical driving conditions. In [32], A new high step-up DC-DC converter topology derived from the Single-Ended Primary Inductor Converter (SEPIC) architecture has been introduced. This configuration incorporates switched-capacitor (SC) networks along with a discontinuous-current quasi-Z-source (qZS) structure to achieve enhanced voltage conversion performance. The proposed converter offers several advantages, including constant output voltage, low voltage stress across semiconductor devices, a wide voltage gain range, and reduced input current ripple. These characteristics make it well-suited for interfacing fuel cells with the inverter DC link in electric vehicles (EVs). Several studies have further explored the integration of fuel cell DC-DC converters with boost converter technologies[9][33][34]. In [33], A Boost Multilevel Cascade Inverter (BMCI) has been proposed as an innovative inverter architecture specifically developed for application in light rail transportation system. This converter achieves a high voltage step-up ratio while maintaining low total harmonic distortion (THD), making it particularly effective for applications that demand voltage amplification from low-voltage energy sources such as battery systems or fuel cells, especially in power electronics interfaces.

In [9], An ultra-high step-up DC-DC converter architecture was introduced, integrating a dual-stage boost structure, coupled inductor technology, and a voltage multiplier cell. This configuration is engineered to deliver substantial voltage amplification, making it suitable for renewable energy applications requiring elevated output levels from low-voltage input source. Similarly, reference [35] presents an enhanced LCC resonant converter design optimized through phase-shift control, offering high efficiency and adaptability. Its wide input and output voltage range makes it particularly well-suited for integration with fuel cell power systems, which typically exhibit significant voltage variability during operation. These studies highlight various advancements in Fuel Cell DC-DC (FDC) converter technology, particularly for electric vehicles (EVs). While numerous designs aim to boosting the input voltage of fuel cells, the selection of best converter for EV applications ultimately depends on the voltage requirements of the vehicle's battery system.

Based on a comprehensive review of the literature [1]-[35], numerous high step-up DC-DC converter topologies have been proposed and analyzed. However, significant research gaps persist, particularly in the application of these converters to renewable energy systems (RES), such as fuel cells (FCs), where the output voltage is typically low and highly variable. Previous studies on improving the voltage gain ratio of high step-up converters through passive circuit modifications, such as the use of double inductors or multiple capacitors, have generally not taken into account the

dynamic response to variations in the fuel cell output voltage, which is highly sensitive to load fluctuations. This condition can result in voltage ripple, voltage instability, and considerable power losses on the load side. Therefore, developing a power conversion strategy that can provide high voltage gain, optimal efficiency, and dynamic stability—while adapting to the inherent characteristics of fuel cells has become an urgent necessity. Furthermore, most existing converters are designed for constant-voltage input conditions. These challenges underscore the need for converter configurations that not only provide substantial voltage gain but also ensure output voltage stability under dynamic load conditions.

The proposed converter topology plays a crucial role in enhancing the reliability of fuel cell–based renewable energy systems while addressing the limitations of existing high step-up DC–DC converters. The novelty of the proposed high step-up DC–DC converter lies in the integration of a Quadratic Boost Converter (QBC) topology with a clamp circuit and a Multiplier Cell (MC), the implementation of an intelligent ANFIS-based control strategy, and the experimental validation of the converter using renewable energy sources particularly a fuel cell that is highly sensitive to load variations. This study analyzes the operational performance of a high step-up DC-DC converter tailored for fuel cell systems, incorporating an intelligent control strategy to ensure precise regulation and stability of the output voltage under dynamic load and input conditions. The system integrates an Adaptive Neuro-Fuzzy Inference System (ANFIS) controller, which enables the converter to maintain a stable voltage output despite fluctuations in load demand. The primary objectives and novel contributions of this research include:

- Achieving a high voltage gain, increasing the fuel cell output voltage by a factor of up to 10;
- Boosting the input voltage from 45 V (typical for FCs) to 400 V, making it suitable for integration with DC bus systems;
- An ANFIS-based control algorithm is implemented to maintain stable output voltage across a wide range of load power variations, thereby improving the overall reliability, dynamic response, and energy conversion efficiency of the fuel cell-based power system

The remainder of this paper is structured as follows: Section II elaborates on the architecture of the proposed system. Section III discusses the proposed methodology and control strategy in detail. Section IV presents the experimental validation and performance evaluation of the system. Finally, Section V concludes the study and outlines directions for future work.

2. Research Method

The converter configuration depicted in Figure 1, features an ultra-high step-up DC-DC topology that integrates a clamp circuit, a multiplier cell (MC), and a quadratic boost converter (QBC). This arrangement functions as a dual-stage boosting mechanism, effectively enhancing the overall voltage conversion ratio. Coupled inductors (CLs) are positioned between the second stage of the boost converter and the multiplier cell. These stages collaboratively enhance the voltage gain, effectively fulfilling the function of a QBC. The combination of the CL and MC significantly contributes to achieving a high step-up voltage. The initial boosting stage includes inductor L_1, diode D_1, switch S_1, and capacitor C_1. Meanwhile, the subsequent boost stage comprises diode D_2, switch S_2, capacitor C_2, and the primary winding (N_1) of the coupled inductor, forming a cascaded configuration to achieve higher voltage gain. The multiplier cell (MC) is constructed using diodes D_{O2} and D_{O3} along with capacitors C_{O2} and C_{O3}, which are interconnected with the secondary winding (N2) of the coupled inductor to further enhance voltage gain. To ensure proper operation, the converter utilizes two power switches (S_1 and S_2) that are operated synchronously. The clamp circuit, consisting of capacitor C_{O1} and diode D_{O1}, serves to suppress voltage spikes caused by switching and minimizes energy loss due to leakage inductance. The coupled inductor is represented by incorporating both magnetizing inductance (L_m) and leakage inductance (L_K) components in its equivalent model. By distributing current between the two inductors (L_1 and the C_L), the converter reduces conduction losses and improves overall efficiency. The specific design parameters of the high step-up DC-DC converter, which is configured to step up the output voltage of the fuel cell to the required DC bus level in Table 1.

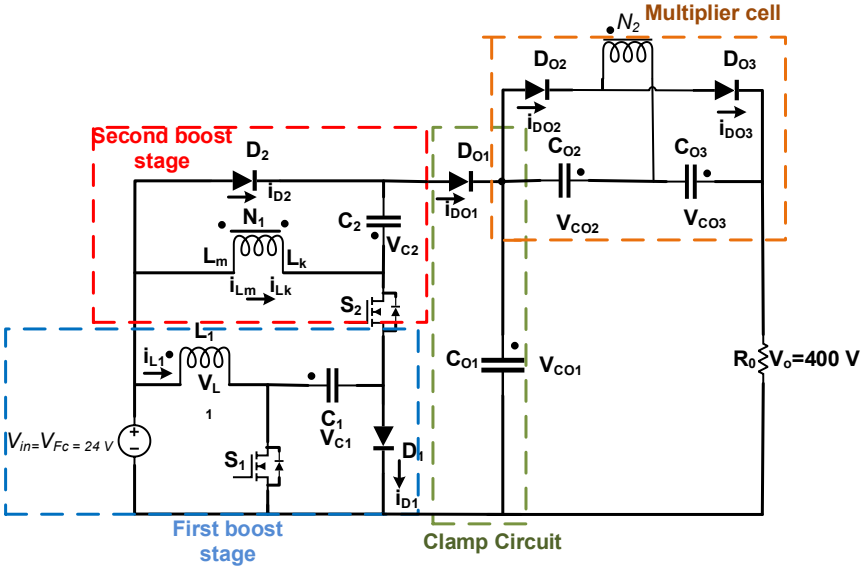

Figure 1. Structure of High Step-up DC-DC Converter

Table 1. Key Parameters of the High Voltage Gain DC-DC Converter Integrated with a Fuel Cell System

Parameter	Value
Input Voltage	40-45V
Output Voltage	400 V
Inductor (L_1)	20 µH
Turn ratio ($n=N_1/N_2$)	12/8
Magnetic inductance (L_m)	200 µH
Leakage inductance (L_k)	1 µH
Capacitors (C_1 and C_2)	45 µF
Output capacitors (C_{O1}, C_{O2} and C_O3)	90 µF
Switching frequency	25 kHz
Resistive load (R)	32-26 ohm

2.1 Operating Mode of Converter

One of the key aspects in evaluating the performance of a high step-up DC-DC converter is its ability to achieve a significant voltage gain. The converter's operation is categorized into five distinct intervals, represented by time instances t_0 through t_5, as illustrated in the waveform diagram in Figure 2 waveform of high step-up DC-DC converter. The corresponding circuit configurations during each operational phase are depicted in Figure 3. These circuit analyses are utilized to investigate and derive the voltage gain characteristics of the converter.

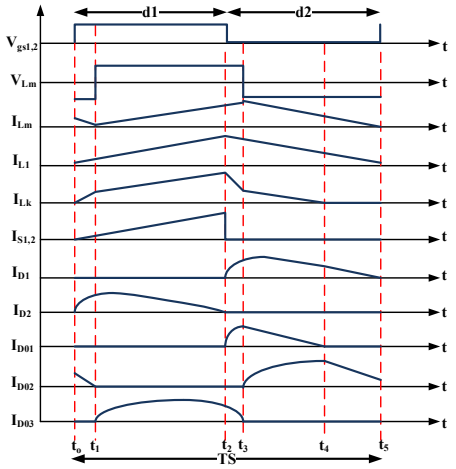

Figure 2. Waveform of High Step-up DC-DC Converter

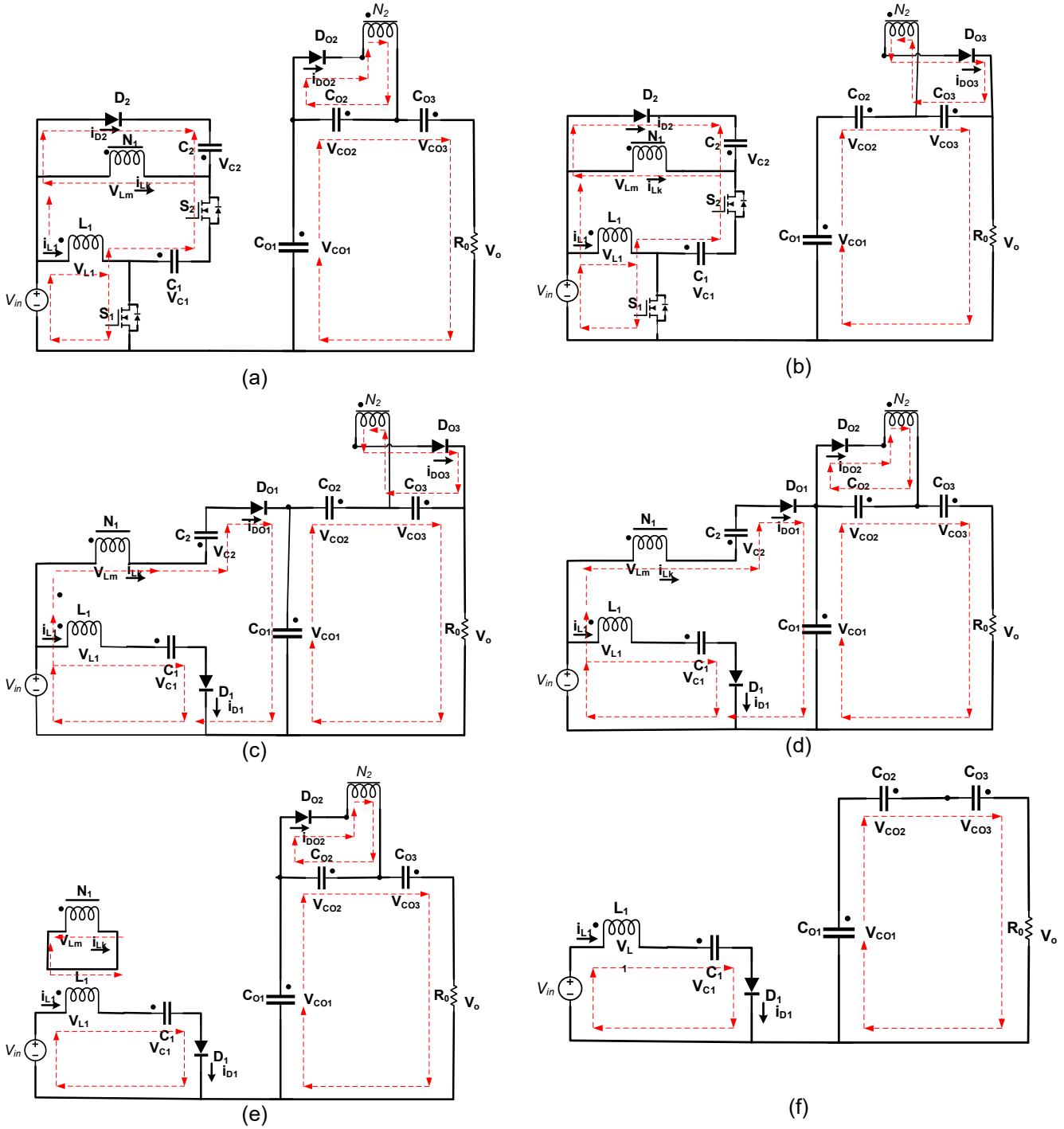

Figure 3. The Operating Behavior of the High Step-up DC-DC Converter Under Continuous Conduction Mode (CCM) is Illustrated as Follows: (a) First Interval Operation from t_0 to t_1, (b) Second Interval from t_1 to t_2, (c) Third Interval from t_2 to t_3, (d) Fourth Interval from t_3 to t_4, and (e) Fifth Interval from t_4 to t_5. In addition, (f) The Fifth Interval is also Analyzed Under Discontinuous Conduction Mode (DCM) Conditions

Operating mode during the first interval *[t_0–t_1]*, as shown in Figure 3(a): During this period, both switches S_1 and S_2 are in the ON state. Diodes D_2 and D_{O2} conduct current, while D_1, D_{O1}, and D_{O3} remain in the OFF state (blocking). The input voltage V_{in} supplies energy to charge inductor L_1, while simultaneously V_{in} and capacitor C_1 charge the magnetizing inductance L_m, leakage inductance L_K, and capacitor C_2, causing the currents through L_m and L_K to increase. Energy stored from the previous cycle is recovered through D_{O2} and used to charge capacitor C_{O2}. During this mode, the output capacitors V_{CO1}, V_{CO2}, and V_{CO3} provide energy to the load.

Operating mode during the second interval [t_1–t_2], as illustrated in Figure 3(b): As a continuation of the first interval, both switches S_1 and S_2 remain in the ON state. Diodes D_2 and D_{O3} conduct, while D_1, D_{O1}, and D_{O2} remain in the OFF (blocking) state. The input voltage V_{in} continues to charge inductor L_1, while V_{in} and capacitor C_1 supply energy to the magnetizing inductance L_m, leakage inductance L_K, and capacitor C_2. During this interval, L_m transfers energy to capacitor C_3 via the secondary winding N_2 of the coupled inductor and diode D_{O3}. Meanwhile, the output capacitors V_{CO1}, V_{CO2}, and V_{CO3} continue to supply energy to the load and gradually discharge until the end of this operating period.

Operating mode during the third interval [t_2–t_3], as shown in Figure 3(c): In this stage, both switches S_1 and S_2 are turned OFF. Diodes D_1, D_{O1}, and D_{O3} are conducting, while D_2 and D_{O2} remain in the OFF state. The input voltage source V_{in}, together with inductor L_1, supplies energy to charge capacitor C_1. At the same time, the magnetizing inductance L_m and leakage inductance L_K begin to discharge, transferring their stored energy to output capacitor C_{O1}. Additionally, the remaining energy in the coupled inductor (CL) is recycled through the secondary winding N_2, diode D_{O3}, and capacitor C_{O2}

Operating mode during the fourth interval [t_3–t_4], as illustrated in Figure 3(d): As a continuation of the previous mode, both switches S_1 and S_2 remain in the OFF state. During this period, diodes D_1, D_{O1}, and D_{O2} are conducting, while D_2 and D_{O3} are in the blocking state. The input voltage V_{in}, along with inductor L_1, continues to charge capacitor C_1. Simultaneously, V_{in}, together with the magnetizing inductance L_m, leakage inductance L_K, and capacitor C_2, delivers energy to C_{O1} via diode D_{O1}. Additionally, L_m transfers energy to C_{O2} through the secondary winding N_2 of the coupled inductor and diode D_{O2}

Operating mode during the fifth interval [t_4–t_5], as shown in Figure 3(e): During this interval, both switches S_1 and S_2 remain in the OFF state. Diodes D_{O1}, D_2, and D_{O3} are not conducting (blocking), while D_1 and D_{O2} remain in the conducting state. The input voltage V_{in}, along with inductor L_1, continues to charge capacitor C_1. At this stage, the leakage inductor current becomes zero (i_{LK} = 0), indicating that no energy is stored or transferred through L_K. The remaining energy in the magnetizing inductor Lm is transferred to capacitor C_{O2} via diode D_{O2}. Meanwhile, the output capacitors V_{CO1}, V_{CO2} and V_{CO3} continue to supply power to the load.

Operating mode during the fifth interval [t_4–t_5] under Discontinuous Conduction Mode (DCM), as illustrated in Figure 3(f): In this mode, all semiconductor components are in the non-conducting (OFF) state, except for diode D_1, which remains conducting. Switches S_1 and S_2, along with diodes D_{O1}, D_{O2}, D_2, and D_{O3}, are in the blocking state. The input voltage V_{in} and inductor L_1 continue to charge capacitor C_1 through diode D_1. At this stage, the currents through both the leakage inductor (i_{LK}) and the magnetizing inductor (i_{Lm}) drop to zero, indicating that no energy is being transferred from these inductive elements. The load is powered solely by the energy stored in the output capacitors V_{CO1}, V_{CO2} and V_{CO3} which continue to discharge to maintain the output voltage.

Equations 1 through 19 are derived based on the equivalent circuit configuration in which D_2 and D_{O3} are conducting, while D_1, D_{O1}, and D_{O2} remain in the blocking state:

$$V_{L1} = V_{in} \tag{1}$$

$$V_{Lm} = kV_{c2} = V_{in} + V_{C1} \tag{2}$$

$$NV_{Lm} = V_{CO3} \tag{3}$$

Based on the corresponding equivalent circuit, the switches are in the OFF state, while diodes D_1, D_{O1}, and D_{O2} are conducting, and all other diodes remain in the blocking state. The subsequent equations are derived under these operating conditions.

$$V_{L1} = V_{in} - V_{C1} \tag{4}$$

$$V_{Lm} = k(V_{in} + V_{C2} - V_{CO1}) \tag{5}$$

$$NV_{Lm} = -V_{CO2} \tag{6}$$

According to the derived relationship, the output voltage is

$$V_o = V_{CO1} + V_{CO2} + V_{CO3} \tag{7}$$

Combining Equations 1 to 6 are consolidated to establish the volt-second balance condition for the inductors during each operational phase, leading to the following mathematical formulations

$$\int_0^{DT_s} V_{in}\,d(t) + \int_{DT_s}^{T_s} (V_{in} - V_{C1})\,d(t) = 0 \tag{8}$$

$$\int_0^{DT_s} kV_{C2}\,d(t) + \int_{DT_s}^{T_s} k(V_{in} - V_{C2} - V_{CO1})\,d(t) = 0 \tag{9}$$

Based on Equations 9, the voltage across capacitor C1 can be expressed as

$$V_{C1} = \frac{V_{in}}{d_2} \tag{10}$$

Substituting Equations 8 into Equations 2, to get voltage of C_2

$$V_{C2} = \frac{(2 - d_1)V_{in}}{d_2} \tag{11}$$

Using Equations 8 and 9 the expression for the voltage across capacitor V_{CO1} is obtained as:

$$V_{CO1} = \frac{(3 - 3d_1 + {d_1}^2)V_{in}}{(d_2)^2} \tag{12}$$

To determine VCO2 Equations 5,11 and 12 are inserted into Equations 6, resulting in the following expression:

$$V_{CO2} = \frac{n\,k\,d_1(2 - d_1)V_{in}}{(d_2)^2} \tag{13}$$

By applying Equations 2 and 11 into Equations 3, the voltage of the final parallel output capacitor (C_{O3}) may be calculated. The outcome is displayed as Equations 14.

$$V_{CO3} = \frac{n\,k\,d_1(2 - d_1)V_{in}}{(d_2)} \tag{14}$$

The output voltage of the converter is obtained by summing the voltages across capacitors C_{O1}, C_{O2}, and C_{O3}, denoted as V_{CO1}, V_{CO2}, and V_{CO3} . Based on this, the converter's voltage gain M and overall output voltage are expressed Equations 15:

$$V_O = \frac{3 + 2\,n\,k - d_1(3 + n\,k - d_1)}{(d_2)^2} V_{in} \tag{15}$$

$$M = \frac{V_O}{V_{in}} = \frac{3 + 2\,n\,k - d_1(3 + n\,k - d_1)}{(d_2)^2} \tag{16}$$

Assuming a perfect magnetic coupling in the coupled inductor (k=1), the voltage gain can be reformulated as follows:

$$M = \frac{V_O}{V_{in}} = \frac{3 + 2\,n - d_1(3 + n\ - d_1)}{(d_2)^2} \tag{17}$$

To ensure practical implementation of the converter, a detailed component design is presented. Under worst-case operating conditions, the minimum inductance values of the inductors are determined to guarantee operation in Continuous Conduction Mode (CCM). Accordingly, based on the converter's analytical model, the minimum inductance values for L_{1min} and L_{mmin} are obtained as expessed in Equations 18 and 19.

$$L_{1min} = \frac{d_1(d_2)^2 R}{2f_s([2 + 2n - d_1(2 + n - d_1)][3 + 2n - d_1(3 + n - d_1)])} \tag{18}$$

$$L_{mmin} = \frac{d_1(2-d_1)(d_2)^2 R}{2f_s[3+2n-d_1(3+n-d_1)]} \quad (19)$$

The design and implementation of the proposed converter are grounded in its targeted performance specifications. These specifications form the basis for developing the ultra-high step-up converter with coupled inductor topology, as detailed in the following design framework. The proposed converter is designed to operate within a defined range of electrical parameters: an input voltage (V_{in}) between 40 and 45 V, a switching frequency (fs) of 25 kHz, a transformer turns ratio (n) of 1.5, an output power (P_o) ranging from 3000 to 6000 W, a load resistance (RRR) between 13 and 82 Ω, and a fixed output voltage (V_o) of 400 V. The worst-case operating condition is identified when the input voltage drops to 40 V while the output power remains at 3000 W, resulting in the most demanding situation for component sizing. To ensure operation in Continuous Conduction Mode (CCM), the minimum inductance values for L_1 and the coupled inductor L_m were determined. Using Equation (40) under extreme duty cycles (D=0.15 and D=0.), the highest required values for L_{1min} and L_{mmin} are calculated as 84 µH and 335 µH, respectively. However, for practical implementation and to provide sufficient margin, the actual inductances selected are L_1=20 µH and L_m=200 µH, which are adequate to maintain CCM across the full range of operating conditions. Capacitor values were derived based on the ripple voltage requirement (ΔV_c=0.01 V) at nominal output conditions of 6000 W, I_o=15 A, and V_o=400 V. The calculated capacitance values are: C_1=17.75 µF, C_2=36.6 µF, C_{O1}=57 µF, C_{O2}=25.7 µF, and C_{O3}=25.8 µF. These values represent the minimum requirements at nominal load. However, since capacitors are subject to performance degradation and variations in operating conditions, it is recommended to design for the worst-case scenario. Accordingly, the capacitor values were increased to C_1 and C_2 is 45 µF and C_{O1}; C_{O2}; C_{O3}; is 90 µF to ensure system stability, suppress output voltage ripple, and enhance overall converter reliability. This design approach guarantees that both inductive and capacitive components are capable of handling transient conditions while maintaining desired output characteristics, thereby ensuring the converter's robust performance across all intended operating scenarios.

2.2 Control System Configuration

The system configuration, illustrated in Figure 4(a), consists of several key components. It incorporates with a fuel cell (FC) serving as a main source. An ANFIS-based control system is implemented in the high step-up DC-DC converter of the FC, which used to maintain a stable output voltage. The proposed control system utilizes the ANFIS algorithm for intelligent regulation. ANFIS integrates fuzzy inference mechanisms with the learning capabilities of neural networks to form a unified intelligent control strategy. Fuzzy Logic Control relies on a membership function and an inference rule base, while ANN control is data-driven and operates through multiple layers. The ANFIS algorithm is further optimized by refining the inference rule base using learning data. The detailed flowchart of the ANFIS controller is presented in Figure 4(b), The flowchart outlines the process of implementing and training an ANFIS controller, which integrates Fuzzy Logic Control and Adaptive Neural Networks.

Collection of Training Data (from FC Output): The process starts by collecting training data, specifically the load voltage output (VLoad). These data are essential to building and training the ANFIS model.

Choose the Fuzzy Data Membership Functions (MFs): Select the MFs and types of MFs to define the fuzzy system. This includes determining an optimization method to refine the membership functions to improve performance. In this controller, there are three membership function inputs which reference of difference error between reference voltage (Vref) and Load voltage output (VLoad)

Application of Fuzzy Inference Rule Base: A fuzzy inference rule base is applied, which provides a logical framework for mapping inputs to outputs based on fuzzy logic principles.

Implementation of the ANFIS Model: The ANFIS model is implemented by combining a fuzzy inference system with the learning capabilities of a neural network.

Error Validation (Is Error > Max Error?): The model checks whether the error (difference between predicted and actual output) exceeds a predefined maximum error threshold. The maximum error tolerance for this learning is 0.0005.

- If **yes**, a new membership function is generated or adjusted to improve performance, and the process loops back.
- If **no**, the model proceeds to the next step.

Training ANFIS: The ANFIS model is trained using the collected data, and its performance is refined iteratively.

Error Acceptance: After training, the system checks whether the error lies within the acceptable range.

- If **yes**, the learning process concludes, and the trained model is finalized.
- If **no**, the model undergoes further training.

Learning Model: Once the error is acceptable, the learning model is complete, and the ANFIS system is ready for deployment.

ANFIS Controller: The trained and optimized ANFIS model is implemented as a controller to regulate the voltage output of Fuel Cell or perform its intended control function.

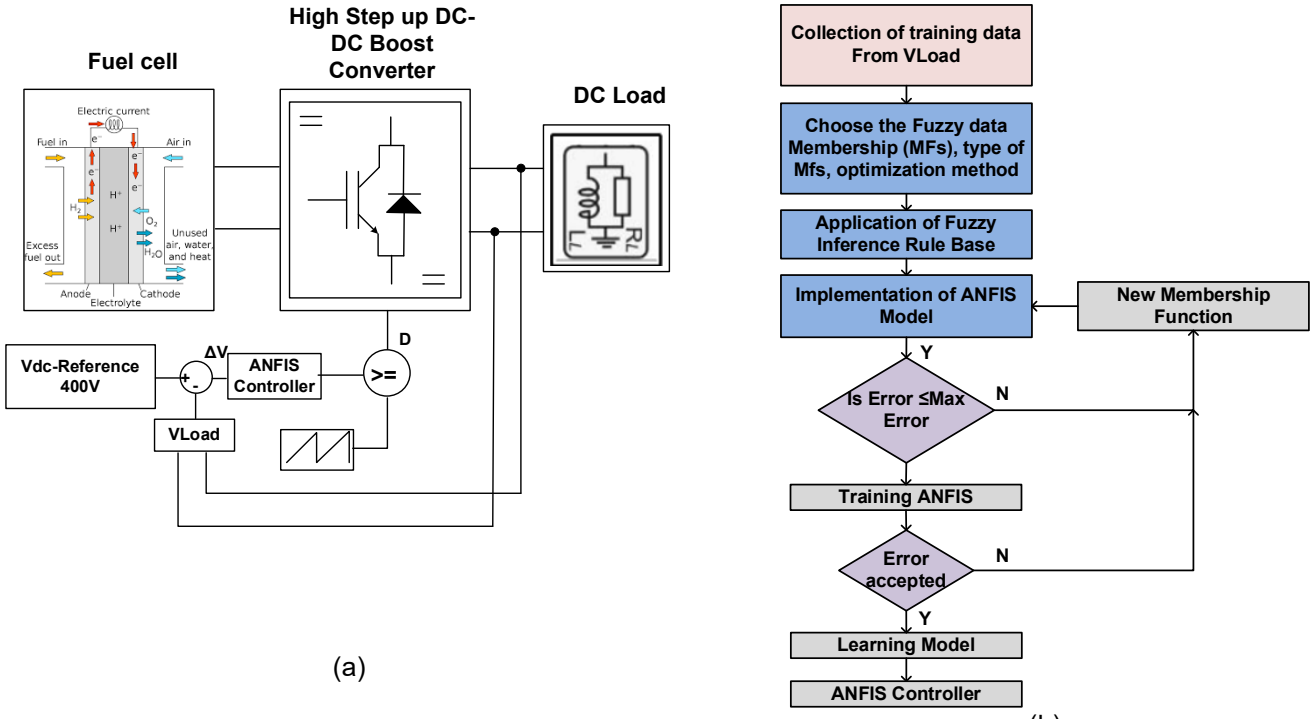

Figure 4. Control System Configuration, (a) Diagram Block System; (b) Flowchart ANFIS Control System

ANFIS receives the voltage deviation (ΔV) as its input, which represents the difference between the reference voltage (Vdc-Reference) and the actual DC bus voltage (VLoad), while its output corresponds to the duty cycle (D). This advanced ANFIS framework combines fuzzy logic with an adaptive learning mechanism that optimizes the membership function parameters to minimize system error effectively. During the training phase, the maximum permissible error tolerance is constrained to 0.0005, and the learning process is conducted over 100 epochs. After completing the tuning of membership parameters, the structure operates as a fully functional ANFIS controller. In the defuzzification stage, a hybrid optimization algorithm is applied to determine the most suitable duty ratio for the high step-up DC–DC converter. The controller consists of a five-layer architecture, and employs three input membership functions. The inference rules are formulated using input–output data pairs and subsequently refined through the backpropagation learning algorithm. Furthermore, the fuzzy inference mechanism is optimized using a trial-and-error approach to efficiently manage uncertainty and nonlinearity in the system

3. Results and Discussion

The comprehensive system evaluation was conducted to assess the reliability of the high step-up DC-DC converter in elevating the low output voltage of the fuel cell. Additionally, the test sought to ensure that the output voltage of converter remained constant despite variations in the load conditions. The system was validated through three cases: (1) variations in the input voltage with constant load power, (2) constant input voltage and load power, and (3) variations in both input and load power.

3.1 Case-1: Variations in the Input Voltage with Constant Load Power

To validate the operational effectiveness and durability of the proposed high step-up DC-DC converter in realistic application scenarios, a validation study was conducted by varying the input voltage while maintaining a fixed output power level. The system was tested under a load of 6000 W, corresponding to the maximum power capacity of the fuel cell (FC) source. During the validation process, the input voltage of the FC was varied within the range of 40 V to 52 V, representing typical fluctuations observed in practical fuel cell systems due to changes in operating temperature, pressure, and hydrogen supply. The converter successfully regulated the output voltage across this input range, producing output voltages between 398 V and 515 V. These results indicate a voltage gain range of approximately 9.6 to 12.9 times, highlighting the converter's ability to operate efficiently even when the fuel cell voltage drops significantly. The system maintained stable operation without triggering overvoltage or undervoltage faults, and the control strategy effectively responded to input variations with minimal output voltage deviation. This demonstrates the converter's capability to accommodate dynamic input conditions while delivering high output voltage, making it suitable for

integration into high-voltage DC bus systems in renewable energy applications. The experiment results are shown in Table 2, with an average gain increase of 9.65 times on the converter. Based on Table 2, The results indicate a linear correlation between the input voltage increment and the corresponding output voltage elevation, where an increase in input voltage is followed by a corresponding increase in output voltage.

Table 2 Gain Voltage of High Step-up DC-DC Converter for FC System

No	V_{input} (V)	V_{output} (V)	Gain
1	52.94	515.64	9.74
2	51.3	499.4	9.73
3	49.9	484.9	9.72
4	48.69	471.63	9.69
5	47.54	459.2	9.66
6	46.45	448	9.64
7	45.45	437.3	9.62
8	44.5	426.9	9.59
9	43.6	417.23	9.57
10	42.76	407.96	9.54
11	41.25	398.8	9.67
	Average Gain		9.65

3.2 Case-2: Constant Input Voltage and Load Power

In the second validation scenario (Case 2), the system was tested under nominal operating conditions, with the fuel cell supplying a constant input voltage of 45 V and the load power maintained at 6000 W, representing the rated capacity of the system. The objective of this experiment was to validate the performance of the ANFIS-based controller in ensuring output voltage stability during steady-state input and load operation, as illustrated in Figure 5. the output voltage remained stable at approximately 400 V throughout the test duration, with minimal deviation from the reference value. The results confirm the efficacy of the ANFIS controller in stabilizing the fuel cell output voltage and achieving high-precision tracking of the setpoint value. The controller was able to mitigate the effects of any transient disturbances and maintain voltage regulation within an acceptable tolerance range, thereby validating its robustness under nominal operation. These findings confirm the suitability of the proposed converter and control system for applications requiring tightly regulated high-voltage DC outputs from variable low-voltage sources such as fuel cells.

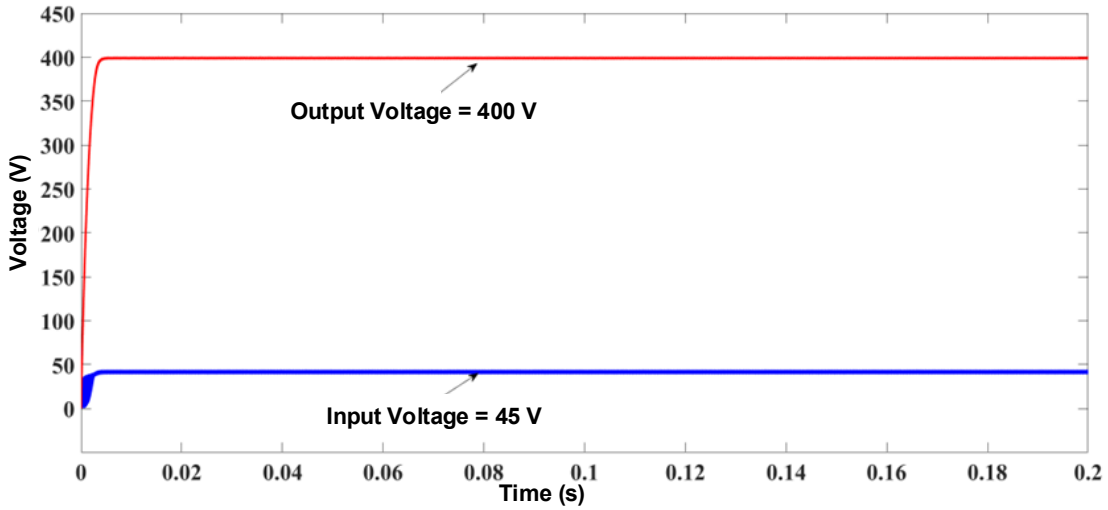

Figure 5. The Input-Output Voltage of High Step-up DC-DC converter for Fuel Cell System

3.3 Case-3: Constant Input Voltage and Variation in Load Power

Case 3 involves validating the dynamic behavior and resilience of the proposed ANFIS-controlled high step-up DC-DC converter under varying load scenarios. The load power was incrementally varied from 1000 W to 6000 W, simulating realistic demand fluctuations commonly encountered in practical applications. Throughout the test, the output voltage remained relatively stable around 400 V, despite significant changes in load demand. This confirms the effectiveness of the integrated ANFIS control strategy in maintaining voltage regulation under dynamic conditions. The controller successfully adapted to each load change, preserving system stability and minimizing voltage deviations.

As illustrated in Figure 6. the output voltage remained within a tight tolerance of ±3.5% of the 400 V reference value, demonstrating the control system's precision in tracking the desired DC bus voltage. The minimum and maximum observed output voltages were 396 V and 410 V, respectively, with the highest voltage recorded at the maximum load of 6000 W. These results validate the ANFIS controller's capability to ensure stable voltage output, even under rapid load variations, thus confirming the system's suitability for applications requiring high reliability and consistent voltage levels—such as fuel cell-powered distributed energy systems and DC microgrids

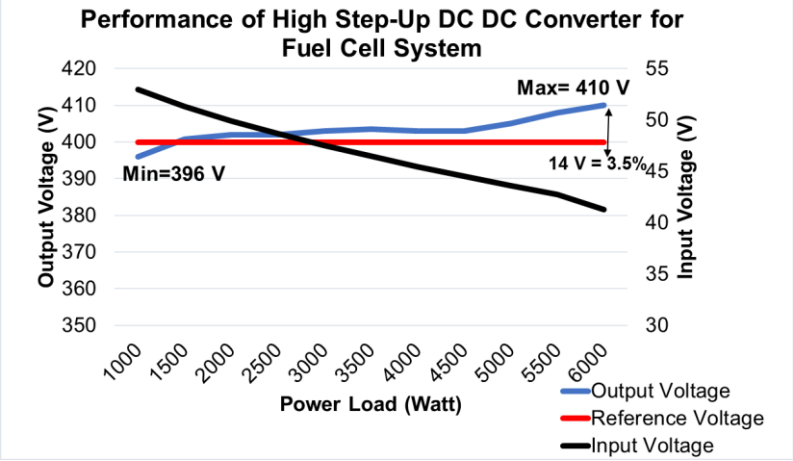

Figure 6. Performance of High Step-up DC-DC Converter for Fuel Cell System

The efficiency performance of the proposed high step-up DC-DC converter was evaluated by analyzing its response to varying load power conditions, ranging from 500 W to 6000 W, as shown in Figure 7. This assessment aimed to determine how the converter's efficiency scales with increasing power demand, a critical factor in the practical deployment of power electronic systems in fuel cell applications. The results indicate a clear trend of increasing efficiency with rising load levels. At lower load conditions, efficiency was relatively modest due to the dominance of switching and conduction losses. However, as the load power increased, the system operated closer to its optimal point, reducing the relative impact of fixed losses and thereby improving overall efficiency. The highest efficiency recorded was **87%**, achieved when the converter operated at the maximum load of **6000 W**. The high efficiency achieved under full-load conditions highlights the capability of the proposed converter topology and control method in effectively reducing power losses, making it suitable for high-power fuel cell systems that require both high voltage gain and energy conversion efficiency

.

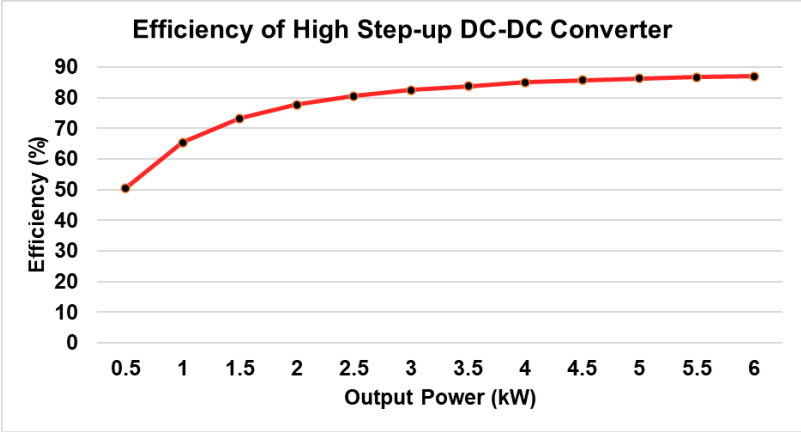

Figure 7. Efficiency of High Step-up DC-DC Converter for Fuel Cell System

3.4 Comparison of the Studied Converter in this Paper and Existing Converter

A comparative analysis is conducted between the proposed topology and several high step-up converters utilizing a Coupled Inductor (CL). The study assesses the quality factors and structural attributes of each converter to confirm the performance and feasibility of the proposed design. The assessment parameters include voltage gain, step-up ratio, component count, efficiency, and output power. Table 3 presents the specifications of the converters described in previous along with the proposed design. While the referenced converters operate under a constant input voltage, the proposed topology integrates a renewable energy source (RES) that produce variable output voltage and combined with an intelligent control system. The focus of this study is on a high step-up converter that evaluates not only voltage gain as the primary comparison parameter but also the overall power-handling capability of the converter

According to the obtained results, the output voltage gain of the proposed converter is higher than that of the other converters. Although the converter presented in [9], [14] can boost the voltage up to 16 times, it is designed for low-power applications with an efficiency of 94%. In comparison, the converter proposed by [32] delivers an output power of 3000 W with an efficiency of 93%, whereas the proposed converter achieves a higher voltage gain with an output power of 6000 W and an efficiency of 87%. Furthermore, the proposed converter integrates an ANFIS-based control system to regulate a relatively constant output voltage and ensure system stability, considering the inherent voltage fluctuations characteristic of fuel cells.

In designing the converter, the component count was maintained within an acceptable range. Generally, achieving a higher voltage conversion ratio demands the inclusion of additional elements due to the complexity of high step-up converter techniques. Nevertheless, the number of components should be minimized to avoid increasing the cost and physical size of the DC–DC converter. Although the proposed converter attains a higher voltage gain, its component count remains comparable to those in [20] and [26]. Compared to the configurations reported by[7] , [21], [25], the proposed design incorporates only about two or four additional components while maintaining structural efficiency. Furthermore, the converters presented in [17] and [32] each utilize two extra components.

Table 3. Comparison of the Studied Converter in this Paper and Existing Converter

Converter	Input voltage level	Output voltage level	Voltage gain	Number of Components	Detail of Components				Full Load Efficiency	Power Output
					Inductors	Capacitors	Power Switches	Diodes		
Proposed converter	45	400	9	14	2	5	2	5	87	6000
[7]	25-80	200	8	12	1	4	2	5	93.1	100
[9]	20	400	20	13	1	5	2	5	94	150
[14]	20-36	600	16	25	6	5	4	10	95	660
[17]	12	180	15	16	6	4	2	4	97	100
[20]	25	400	16	14	2	5	2	5	94	150
[21]	24-36	400	12	10	2	3	2	3	92	300
[22]	10	100	10	15	3	5	1	6	90	100
[25]	40	250	6.25	8	1	2	2	3	-	200
[26]	48	650	13	14	2	5	2	5	90	200
[32]	100-300	800	8	16	3	7	1	5	95	3000

4. Conclusion

This paper explores the implementation of an ANFIS control system for enhancing the performance of high step-up DC-DC converter integrated with a FC system. The proposed high step-up converter features a novel structural configuration that integrates a clamp unit, a Voltage Multiplier Cell (VMC), and cascaded Quadratic Boost Converter (QBC) stages. The contribution of this converter topology lies in its ability to enhance the reliability of fuel cell–based renewable energy systems, achieve high voltage amplification, ensure optimal efficiency, and maintain dynamic stability. The modeling, control structure, and detailed analysis were thoroughly discussed. The converter is engineered to boost the fuel cell's low-voltage output from 45 V to 400 V, enabling integration with high-voltage DC bus systems. The ANFIS control system is employed to control the output voltage, ensuring stability even under highly variable conditions of the fuel cell system. Test results confirm that the control system effectively maintains a stable DC bus voltage without overshoot, despite fluctuations in power loads. The voltage deviation between the DC-bus reference voltage and the output voltage remains within a 3.5% tolerance. Additionally, the converter achieves an efficiency of up to 87% under load conditions. Future research could explore alternative converter configurations and artificial intelligence-based control systems, with a focus on hardware implementation.

Acknowledgement

The authors are grateful to Universitas Semarang in Semarang – Indonesia for supporting this research.

References

[1] M. Meraj, M. S. Bhaskar, B. P. Reddy, and A. Iqbal, "Non-Isolated DC-DC Power Converter with High Gain and Inverting Capability," *IEEE Access*, vol. 9, pp. 62084–62092, 2021. https://doi.org/10.1109/ACCESS.2021.3074459

[2] M. J. Sanjari, H. B. Gooi, and N. K. C. Nair, "Power generation forecast of hybrid PV-Wind system," *IEEE Trans Sustain Energy*, vol. 11, no. 2, pp. 703–712, Apr. 2020. https://doi.org/10.1109/TSTE.2019.2903900

[3] M. Manohar, E. Koley, and S. Ghosh, "Stochastic Weather Modeling-Based Protection Scheme for Hybrid PV-Wind System with Immunity against Solar Irradiance and Wind Speed," *IEEE Syst J*, vol. 14, no. 3, pp. 3430–3439, Sep. 2020. https://doi.org/10.1109/JSYST.2020.2964990

[4] Z. Saadatizadeh, P. C. Heris, X. Liang, and E. Babaei, "Expandable Non-Isolated Multi-Input Single-Output DC-DC Converter with High Voltage Gain and Zero-Ripple Input Currents," *IEEE Access*, vol. 9, pp. 169193–169219, 2021. https://doi.org/10.1109/ACCESS.2021.3137126

[5] M. Zhang, Z. Wei, M. Zhou, F. Wang, Y. Cao, and L. Quan, "A High Step-Up DC–DC Converter With Switched-Capacitor and Coupled-Inductor Techniques," *IEEE Journal of Emerging and Selected Topics in Industrial Electronics*, vol. 3, no. 4, pp. 1067–1076, 2022. https://doi.org/10.1109/jestie.2022.3173909

[6] J. Y. Kim, B. S. Lee, Y. J. Lee, and J. K. Kim, "Integrated Multi Mode Converter With Single Inductor for Fuel Cell Electric Vehicles," *IEEE Transactions on Industrial Electronics*, vol. 69, no. 11, pp. 11001–11011, 2022. https://doi.org/10.1109/TIE.2021.3118390

[7] X. Wu, M. Yang, M. Zhou, Y. Zhang, and J. Fu, "A Novel High-Gain DC-DC Converter Applied in Fuel Cell Vehicles," *IEEE Trans Veh Technol*, vol. 69, no. 11, pp. 12763–12774, 2020. https://doi.org/10.1109/TVT.2020.3023545

[8] S. Hasanpour, M. Forouzesh, Y. Siwakoti, and F. Blaabjerg, "A New High-Gain, High-Efficiency SEPIC-Based DC–DC Converter for Renewable Energy Applications," *IEEE Journal of Emerging and Selected Topics in Industrial Electronics*, vol. 2, no. 4, pp. 567–578, 2021. https://doi.org/10.1109/jestie.2021.3074864

[9] M. Rezaie and V. Abbasi, "Ultrahigh Step-Up DC-DC Converter Composed of Two Stages Boost Converter, Coupled Inductor, and Multiplier Cell," *IEEE Transactions on Industrial Electronics*, vol. 69, no. 6, pp. 5867–5878, 2022. https://doi.org/10.1109/TIE.2021.3091916

[10] A. Rajabi, A. Rajaei, V. M. Tehrani, P. Dehghanian, J. M. Guerrero, and B. Khan, "A Non-Isolated High Step-Up DC-DC Converter Using Voltage Lift Technique: Analysis, Design, and Implementation," *IEEE Access*, vol. 10, pp. 6338–6347, 2022. https://doi.org/10.1109/ACCESS.2022.3141088

[11] B. Sri Revathi and M. Prabhakar, "Solar PV fed DC Microgrid: Applications, Converter Selection, Design and Testing," *IEEE Access*, 2022. https://doi.org/10.1109/ACCESS.2022.3199701

[12] M. Badiane, P. A. A. Honadia, B. Zouma, and F. I. Barro, "Quadratic Boost Converter: An Analysis with Passive Components Losses," *Open Journal of Applied Sciences*, vol. 11, no. 02, pp. 202–215, 2021. https://doi.org/10.4236/ojapps.2021.112014

[13] S. Vemparala Rao and K. Sundaramoorthy, "Performance Analysis of Voltage Multiplier Coupled Cascaded Boost Converter With Solar PV Integration for DC Microgrid Application," *IEEE Trans Ind Appl*, vol. 59, no. 1, pp. 1013–1023, Jan. 2023. https://doi.org/10.1109/TIA.2022.3209616

[14] A. Gupta, N. Korada, and R. Ayyanar, "Quadratic-Extended-Duty-Ratio Boost Converters for Ultra High Gain Application With Low Input Current Ripple and Low Device Stress," *IEEE Trans Ind Appl*, vol. 59, no. 1, pp. 938–948, 2023. https://doi.org/10.1109/TIA.2022.3207132

[15] T. Shanthi, S. U. Prabha, and K. Sundaramoorthy, "Non-Isolated n-Stage High Step-up DC-DC Converter for Low Voltage DC Source Integration," *IEEE Transactions on Energy Conversion*, vol. 36, no. 3, pp. 1625–1634, 2021. https://doi.org/10.1109/TEC.2021.3050421

[16] B. Zhu, S. Chen, Y. Zhang, and Y. Huang, "An Interleaved Zero-Voltage Zero-Current Switching High Step-Up DC-DC Converter," *IEEE Access*, vol. 9, pp. 5563–5572, 2021. https://doi.org/10.1109/ACCESS.2020.3048387

[17] A. Asghari and Z. J. Yegane, "A High Step-Up DC-DC Converter with High Voltage Gain and Zero-Voltage Transition," *IEEE Transactions on Industrial Electronics*, vol. 71, no. 7, pp. 6946–6954, 2024. https://doi.org/10.1109/TIE.2023.3312434

[18] F. Liu, G. Zhou, X. Ruan, S. Ji, Q. Zhao, and X. Zhang, "An Input-Series-Output-Parallel Converter System Exhibiting Natural Input-Voltage Sharing and Output-Current Sharing," *IEEE Transactions on Industrial Electronics*, vol. 68, no. 2, pp. 1166–1177, 2021. https://doi.org/10.1109/TIE.2020.2967669

[19] H. N. Tran, T. T. Le, H. Jeong, S. Kim, and S. Choi, "A 300 kHz, 63 kW/L ZVT DC-DC Converter for 800-V Fuel Cell Electric Vehicles," *IEEE Trans Power Electron*, vol. 37, no. 3, pp. 2993–3006, 2022. https://doi.org/10.1109/TPEL.2021.3108815

[20] V. Abbasi, N. Talebi, M. Rezaie, A. Arzani, and F. Y. Moghadam, "Ultrahigh Step-Up DC-DC Converter Based on Two Boosting Stages With Low Voltage Stress on Its Switches," *IEEE Transactions on Industrial Electronics*, vol. 70, no. 12, pp. 12387–12398, 2023. https://doi.org/10.1109/TIE.2023.3236064

[21] C. H. Lin, M. S. Khan, J. Ahmad, H. D. Liu, and T. C. Hsiao, "Design and Analysis of Novel High-Gain Boost Converter for Renewable Energy Systems (RES)," *IEEE Access*, vol. 12, no. February, pp. 24262–24273, 2024. https://doi.org/10.1109/ACCESS.2024.3365705

[22] R. Rahimi, S. Habibi, M. Ferdowsi, and P. Shamsi, "An Interleaved High Step-Up DC-DC Converter Based on Integration of Coupled Inductor and Built-in-Transformer with Switched-Capacitor Cells for Renewable Energy Applications," *IEEE Access*, vol. 10, pp. 34–45, 2022. https://doi.org/10.1109/ACCESS.2021.3138390

[23] S. Khan, M. Zaid, A. Mahmood, J. Ahmad, and A. Alam, "A Single Switch High Gain DC-DC converter with Reduced Voltage Stress," *7th IEEE Uttar Pradesh Section International Conference on Electrical, Electronics and Computer Engineering, UPCON 2020*, pp. 5–10, 2020. https://doi.org/10.1109/UPCON50219.2020.9376578

[24] T. Rahimi, L. Ding, H. Gholizadeh, R. S. Shahrivar, and R. Faraji, "An Ultra High Step-Up DC-DC Converter Based on the Boost, Luo, and Voltage Doubler Structure: Mathematical Expression, Simulation, and Experimental," *IEEE Access*, vol. 9, pp. 132011–132024, 2021. https://doi.org/10.1109/ACCESS.2021.3115259

[25] M. Ashok Bhupathi Kumar and V. Krishnasamy, "Quadratic Boost Converter with Less Input Current Ripple and Rear-End Capacitor Voltage Stress for Renewable Energy Applications," *IEEE J Emerg Sel Top Power Electron*, vol. 10, no. 2, pp. 2265–2275, 2022. https://doi.org/10.1109/JESTPE.2021.3122354

[26] T. Vysagh and S. Kumaravel, "Quadratic Gain-Based Boost Converter: Reduced Switch Current and Component Voltage Stress," *2023 IEEE International Conference on Energy Technologies for Future Grids, ETFG 2023*, pp. 1–6, 2023. https://doi.org/10.1109/ETFG55873.2023.10408490

[27] H. Tarzamni, N. V. Kurdkandi, H. S. Gohari, M. Lehtonen, O. Husev, and F. Blaabjerg, "Ultra-High Step-Up DC-DC Converters Based on Center-Tapped Inductors," *IEEE Access*, vol. 9, pp. 136373–136383, 2021. https://doi.org/10.1109/ACCESS.2021.3117856

[28] B. Barik, D. Srinivasan, K. Arulvendhan, and N. Suresh, "High step-up DC-DC Converter based Renewable Energy System for Improving Power Quality and Low Voltage Stress using PI Controller Technique," *International Conference on Edge Computing and Applications, ICECAA 2022 - Proceedings*, no. Icecaa, pp. 698–704, 2022. https://doi.org/10.1109/ICECAA55415.2022.9936547

[29] Y. Zhang, S. Member, G. Spiazzi, S. Buso, and T. Caldognetto, "MIMO Control of a High-Step-Up Isolated Bidirectional DC – DC Converter," vol. 69, no. 5, pp. 4687–4696, 2022. https://doi.org/10.1109/TIE.2021.3078393

[30] M. Veerachary and N. Kumar, "Analysis and Design of Quadratic following Boost Converter," *IEEE Trans Ind Appl*, vol. 56, no. 6, pp. 6657–6673, 2020. https://doi.org/10.1109/TIA.2020.3021363

[31] S. Naresh, S. Peddapati, and M. L. Alghaythi, "A Novel High Quadratic Gain Boost Converter for Fuel Cell Electric Vehicle Applications," *IEEE Journal of Emerging and Selected Topics in Industrial Electronics*, vol. 4, no. 2, pp. 637–647, 2023. https://doi.org/10.1109/jestie.2023.3248449

[32] N. Elsayad, H. Moradisizkoohi, and O. Mohammed, "A New SEPIC-Based Step-Up DC-DC Converter with Wide Conversion Ratio for Fuel Cell Vehicles: Analysis and Design," *IEEE Transactions on Industrial Electronics*, vol. 68, no. 8, pp. 6390–6400, 2021. https://doi.org/10.1109/TIE.2020.3007110

[33] I. Krastev and P. Tricoli, "Boost Multilevel Cascade Inverter for Hydrogen Fuel Cell Light Railway Vehicles," *IEEE Transactions on Industrial Electronics*, vol. 69, no. 8, pp. 7837–7847, 2022. https://doi.org/10.1109/TIE.2021.3105992

[34] N. Agrawal, S. Samanta, and S. Ghosh, "Optimal State Feedback-Integral Control of Fuel-Cell Integrated Boost Converter," *IEEE Transactions on Circuits and Systems II: Express Briefs*, vol. 69, no. 3, pp. 1382–1386, 2022. https://doi.org/10.1109/TCSII.2021.3117716

[35] S. H. Son *et al.*, "Optimal Design of LCC Resonant Converter With Phase Shift Control for Wide Input/Output Voltage Ranges in Fuel Cell System," *IEEE Transactions on Industrial Electronics*, vol. 71, no. 4, pp. 3537–3547, 2024. https://doi.org/10.1109/TIE.2023.3279549